JCTC Journal of Chemical Theory and Computation

Article

pubs.acs.org/JCTC

Two-Photon Absorption of Metal-Assisted Chromophores

Xin Li,*[,†] Zilvinas Rinkevicius,[†,‡] and Hans Ågren[†]

[†]Division of Theoretical Chemistry & Biology, School of Biotechnology, KTH Royal Institute of Technology, SE-10691 Stockholm, Sweden

[‡]Swedish e-Science Research Centre, KTH Royal Institute of Technology, SE-10044 Stockholm, Sweden

Supporting Information

ABSTRACT: Aiming to understand the effect of a metal surface on nonlinear optical properties and the combined effects of surface and solvent environments on such properties, we present a multiscale response theory study, integrated with dynamics of the two-photon absorption of 4-nitro-4′-amino-*trans*-stilbene physisorbed on noble metal surfaces, considering two such surfaces, Ag(111) and Au(111), and two solvents, cyclohexane and water, as cases for demonstration. A few conclusions of general character could be drawn: While the geometrical change of the chromophore induced by the environment was found to notably alter (diminish) the two-photon absorption cross section in the polar medium, the effects of the metal surface and solvent on the electronic structure of the chromophore surpasses the geometrical effects and leads to a considerably enhanced two-photon absorption cross section in the polar solvent. This enhancement of two-photon absorption arises essentially from the metal charge image induced enlargement of the difference between the dipole moment of the excited state and the ground state. The orientation-dependence of the two-photon absorption is found to connect with the lateral rotation of the chromophore, where the two-photon absorption reaches its maximum when the polarization of the incident light coincides with the long-axis of the chromophore. Our results demonstrate a distinct enhancement of the two-photon absorption by a metal surface and a polar medium and envisage the employment of metal−chromophore composite materials for future development of nonlinear optical materials with desirable properties.

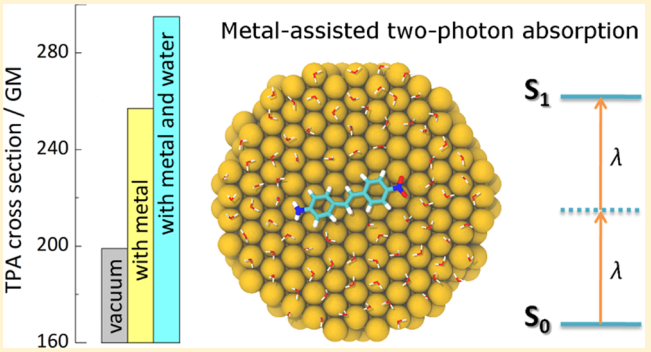

INTRODUCTION

Composite materials containing organic chromophores and metal nanoparticles are generally considered to be promising candidates for practical applications as nonlinear optical (NLO) nanodevices, owing to the combination of the NLO performance of the organic chromophores and some salient physical properties of the inorganic counterparts. The metal nanoparticles provide ordered orientation of the adsorbed chromophores and a local field enhancement for the NLO response—two characteristics that are advantageous for the construction of devices with combined functionality. In case of chemisorption, the optical properties of the adsorbents can be altered by direct binding with metal surface/nanoparticles through charge transfer, electron sharing, or hybridization of molecular orbitals between the metal cluster and the chromophore; while in case of physisorption, metal surface/nanoparticles put indirect effects through geometrical relaxation of the adsorbed chromophore as well as direct polarization effects on the electronic structure of the adsorbent. These effects provide signal changes and facilitate detection of events taking place in the adsorbent, and rational design of such NLO hybrids thus requires insight into the underlying mechanisms regarding the effects of molecular geometry, electronic structure, and environment on the optical properties of the organic NLO chromophores, something that in turn calls for theoretical modeling. In particular, the direct polarization effects of a metal surface on the optical properties of physisorbed chromophores as well as the indirect effects on their geometries have been successfully tackled by a combined molecular dynamics (MD) and multiscale quantum mechanical/molecular mechanical (QM/MM) approach.[1−3] It is our aim in this paper to further expand the approach to theoretical evaluation of the two-photon absorption (TPA) of metal-assisted chromophores.

Among NLO properties, TPA is of particular interest owing to several outstanding characteristics making this process apt for applications in widely different areas like data-storage, optical limiting, up-converted lasing, and biophotonics.[4] Compared with one-photon absorption it offers low destructive excitation of biocompatible chromophores *in vivo*, low scattering, and deep penetration into tissue. This follows from the fact that TPA provides access to an excited state through photons of half the excitation energy, that intensity losses due to absorption and scattering are minimized, and that biological samples therefore are subject to a lower risk of being

Received: July 6, 2014

   dx.doi.org/10.1021/ct500579n | J. Chem. Theory Comput. XXXX, XXX, XXX−XXX

damaged by the light irradiation. As such, chromophores with large TPA cross-section at certain wavelengths are highly desirable. The purpose of this paper is to investigate how the TPA cross-section of chromophores is modulated through adsorption onto metallic surfaces or nanoparticles.

Due to the large, generally complex, environment of the NLO chromophores, it is impractical to describe the whole system with great detail by means of pure quantum mechanical approaches. Multiscale modeling methods provide a practical solution by combining classical physics and quantum physics and taking advantage of a hierarchical description of the system with different levels of theories. Such modeling is conducted by splitting the system into a quantum mechanical (QM) region surrounded by a molecular mechanical (MM) region; the former is treated by the high-level QM methods, while the latter is described by a polarizable medium[5] or atomistic particles with predefined electrostatics, induction, dispersion, short-range repulsion, etc. This integrated approach has been proven powerful in treating many types of extended systems with complex environments, providing structures, dynamics, and properties at the atomistic resolution.[6,7] While so far such multiscale approaches mostly have been applied with organic embedding, hybrid QM/MM simulations with metallic embedding are attractive because organometallic-based nanodevices exhibit unique capabilities for a wide range of applications, like single molecule sensing, imaging, and energy conversion.

The development of hybrid quantum−classical approaches for modeling metal−chromophore complexes involves the polarizable continuum model,[8] heterogeneous solvation response theory,[9] finite-difference time-domain approach,[10] polarizable QM/MM,[11] image charge augmented QM/MM,[12] and the discrete interaction model/quantum mechanics model.[13,14] Based on the capacitance−polarization interaction model,[15] we have developed the QM/MM linear and quadratic response theory with metallic embedding, coined as the QM/CMM model,[1] which enables direct assessment of the structure−response−functionality relationship of physisorbed chromophores on metal surfaces or nanoparticles. So far the QM/CMM approach has been applied in multiscale modeling of absorption,[1] circular dichroism,[2] and second harmonic generation properties[3] of physisorbed chromophores on gold surfaces. In this paper, we extend its application to the two-photon processes and discuss the effect of metallic surfaces for that process, using 4-nitro-4′-amino-*trans*-stilbene (NATSB) as a model compound and gold and silver crystals as metal substrates. The NATSB compound contains a *trans*-stilbene unit as π-bridge connecting the electron-donating $-NH_2$ group and the electron-withdrawing $-NO_2$ group, forming a D-π-A structure. The *trans*-stilbene unit is a very common building block for TPA chromophores, and the D-π-A architecture shows charge transfer character which is sensitive to polarization effects of the environment due to its nonvanishing dipole moment.[16] In addition, NATSB is a small molecule containing 30 atoms, which is suitable for extensive simulations and quantum chemical calculations. NATSB is thus expected to serve as a model compound for theoretical studies of the effects of metal surfaces on the TPA cross section.

COMPUTATIONAL DETAILS

Molecular Dynamics Simulations. In our previous studies we have employed a sequential approach to investigate the statistically averaged spectra of metal-assisted chromophores, that is, MD simulations followed by multiscale QM/MM calculations. The calculated properties were averaged over a series of uncorrelated snapshots from MD trajectory so that they correspond to experimental observations. Encouraged by the successful applications of such sequential MD and QM/MM approach, we in this work employed MD simulations to model the adsorption dynamics of NATSB on gold and silver surfaces, where the CHARMM general force field (CGenFF)[17] and the GolP-CHARMM[18] and AgP-CHARMM[19] extensions are used to model the NATSB molecule, gold surface, and silver surface, respectively. Here the CGenFF parameters for the NATSB molecule have been refined to reproduce the QM-optimized geometry and rotational barriers of the dihedral angles (see the Supporting Information for details). The GolP-CHARMM and AgP-CHARMM extensions to the CHARMM force field are developed by Walsh and co-workers toward realistic modeling of gold and silver surfaces with the image charge effects taken into account by a rigid dipole approach.[18] In addition, water and cyclohexane were employed as solvent to model polar and apolar environments, respectively. We employed the TIP3P-CHARMM water model[20] and the CGenFF parameters for cyclohexane. The Ag(111) and Au(111) surfaces were constructed as six-layered slabs, with the exposed areas in the rectangular simulation box amounting to 34.98 × 34.62 Å^2 for gold and 35.03 × 34.67 Å^2 for silver, respectively. For both surfaces, the z-dimension of the simulation box is set at around 70 Å to minimize the interaction between the surface and its periodic images. Each simulation was conducted under *NVT* ensemble for 10 ns with the temperature maintained at 298 K by the velocity-rescaling algorithm[21] as implemented in the GROMACS program package[22] (version 4.5.2), and 80 snapshots were evenly extracted from the trajectory of the last 4 ns.

QM/CMM Calculations. From each snapshot the model system was constructed as the input for subsequent QM/CMM calculations by trimming the metallic substrate as a three-layered cylinder with a cutoff radius of 15 Å together with the solvent molecules on top of the surface within a height of 20 Å. Our experience suggests that such a truncated model is sufficient to model the environment effects arising from the metal surface and surrounding solvent molecules.[2] We employed the range-separated CAM-B3LYP functional[23] and the def-TZVP set[24] for the QM region, the capacitance−polarization interaction model for gold and silver with parameters from the literature,[13] and discrete point charges as in TIP3P-CHARMM and CGenFF for solvent molecules. Sałek et al. reported that the quadratic response formulation of TPA by density functional theory provides comparable results with coupled-cluster response calculations.[25] The use of the def-TZVP basis set has been shown to provide excitation energies and TPA cross sections very close to the 6-311++G(3df,3pd) basis set at a shorter computational time.[26] The QM/CMM calculations were conducted using the DALTON quantum chemistry program package.[27]

The TPA transition amplitude tensor $\boldsymbol{S}$ of the chromophore was calculated assuming that the energy of the incoming photon is equal to half of the ground-state-to-excited-state excitation energy

$$S_{\alpha\beta} = \sum_{k>0} \left(\frac{\langle 0|\hat{\mu}_\alpha|k\rangle\langle k|\hat{\mu}_\beta|f\rangle}{\omega_k - \omega_f/2} + \frac{\langle 0|\hat{\mu}_\beta|k\rangle\langle k|\hat{\mu}_\alpha|f\rangle}{\omega_k - \omega_f/2} \right) \quad (1)$$

dx.doi.org/10.1021/ct500579n | J. Chem. Theory Comput. XXXX, XXX, XXX−XXX

where α and β denote Cartesian components, and 0, k, and f denote the ground state, the intermediate state, and the final excited state, respectively. The observed TPA cross section is dependent on the polarization direction of the incoming photons, and the corresponding isotropic average of TPA transition probability (in atomic unit) is given by[28]

$$\delta^{\mathrm{au}} = \frac{1}{30}\sum_{\alpha\beta}\left(FS_{\alpha\alpha}S_{\beta\beta} + GS_{\alpha\beta}S_{\alpha\beta} + HS_{\alpha\beta}S_{\beta\alpha}\right) \quad (2)$$

where F, G, and H are variables that are dependent on the polarization vectors of the incoming photons. In the case of two identical linearly polarized photons, these three variables are all equal to two.[28] The TPA transition probability can then be converted to TPA cross section assuming Lorentzian broadening and a width Γ of 0.0037 au (equivalent to 0.1 eV)

$$\sigma^{\mathrm{TPA}} = \frac{(2\pi)^3\alpha a_0^5\omega^2}{c\pi\Gamma}\delta^{\mathrm{au}} \quad (3)$$

where α is the fine structure constant ($7.2973525698 \times 10^{-3}$), a_0 is the Bohr radius ($5.291772108 \times 10^{-9}$ cm), ω is the energy of incoming photon in atomic unit, c is the speed of light in vacuum ($2.99792458 \times 10^{10}$ cm/s), and Γ is the broadening width. For Γ we choose the standard value of 0.1 eV. The metal surfaces may put an effect on the lifetime of the excited state and the choice of Γ, which, however, is beyond the scope of this study. In this paper, we focus on the direct polarization effects of metal surfaces and solvent molecules on TPA cross section of the NATSB chromophore.

RESULTS AND DISCUSSION

Absorption on Metal Surfaces. The adsorption of NATSB on metal surfaces is monitored by the vertical distances of its four groups with respect to the surface, i.e. the $-NO_2$ group, the $-NH_2$ group, and the two phenyl rings. As shown in Figure 1, NATSB adopts different geometries

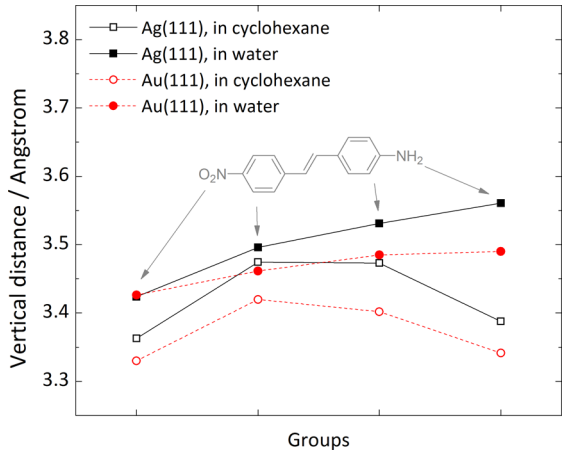

Figure 1. Vertical distances of the nitrogen atoms and phenyl rings of NATSB with respect to metal surfaces.

when interacting with different metal surfaces and solvent molecules. In particular, it adopts a bent conformation when an apolar solvent like cyclohexane is used to solvate the system, where the peripheral $-NO_2$ and $-NH_2$ groups stay closer to the surface with the two phenyl rings at slightly larger vertical distances from the surface. When polar solvent molecules like water are present, NATSB adopts a more linear conformation with its $-NO_2$ groups residing closer to the surface and the $-NH_2$ groups slightly tilted up. In general, the NATSB molecules show a greater affinity to the Au(111) surface over the Ag(111) surface, in accordance with the literature reports that gold is mostly favored over silver for adsorption of amino acids.[19]

The different adsorption geometries lead to different behavior in the lateral rotation of the NATSB molecule. Figure 2 shows time-evolution of the angle between the $NO_2 \rightarrow NH_2$

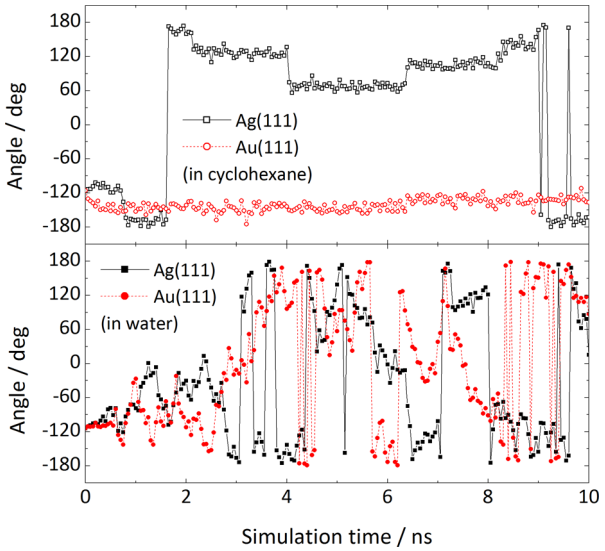

Figure 2. Time-evolution of the angle between the $NO_2 \rightarrow NH_2$ vector of NATSB and the x-axis.

vector of NATSB and the x-axis, which describes the rotation of the molecule around the normal direction of the metal surface, i.e. the z-axis. A distinct rotational behavior was observed between the polar solvent and the apolar solvent, which is consistent with the adsorption distances shown in Figure 1. When the system is solvated by polar cyclohexane, the molecule adopts a bent conformation with the $-NO_2$ and $-NH_2$ groups close to the surface, and consequently the lateral rotation of the molecule becomes very slow owing to the strong interaction between the surface and NATSB. In particular, the NATSB molecule behaves as if it is "anchored" on the Au(111) surface with very little variation in the angle between the $NO_2 \rightarrow NH_2$ vector and the x-axis. On the Ag(111) surface the angle experiences several stepwise changes, still the variation is very limited. Differently, when the system is solvated by water molecules, the NATSB molecule is able to span the whole $[-180°, 180°]$ interval within a few nanoseconds, owing to the increased distance and diminished interaction between the molecule and the surfaces. Such different behavior in lateral rotation is expected to result in distinct characteristics in the orientation-dependent NLO properties.

Dipole Strengths and Excitation Energies. For each snapshot extracted from the MD trajectory, we employed three different models for quantum mechanical calculations of one- and two-photon absorption: (i) NATSB in vacuum, (ii) NATSB with metal surface, and (iii) NATSB with metal surface and surrounding solvent molecules. Averaging over the 80 snapshots provides a statistical description of one- and two-photon absorption properties, and the effects of the metal surfaces and solvent molecules can be clarified through comparison among the results obtained from the three models

dx.doi.org/10.1021/ct500579n | J. Chem. Theory Comput. XXXX, XXX, XXX−XXX

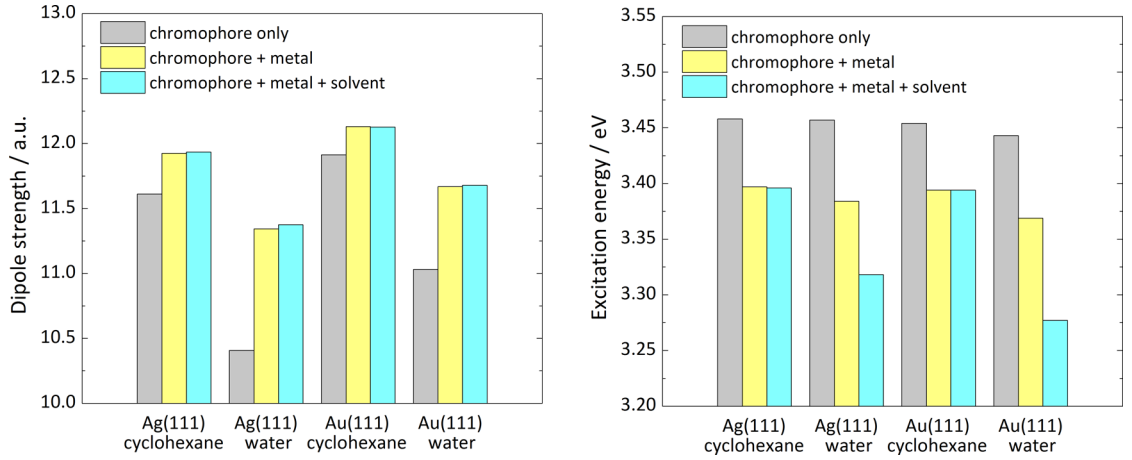

Figure 3. Computed (left) dipole strengths and (right) excitation energies by different models: chromophore only, chromophore + metal, and chromophore + metal + solvent.

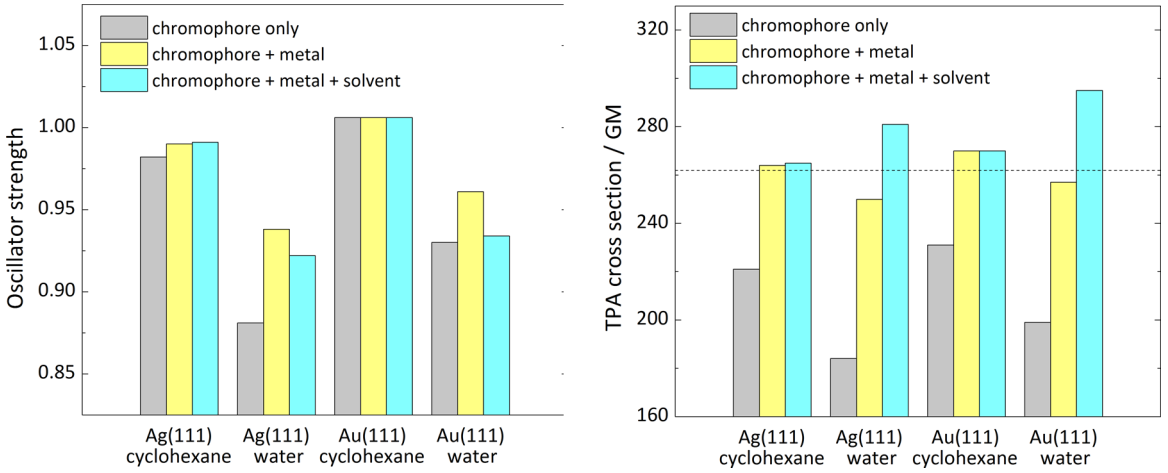

Figure 4. Computed (left) one-photon absorption oscillator strengths and (right) two-photon absorption cross sections by different models: chromophore only, chromophore + metal, and chromophore + metal + solvent.

with different treatment of environment effects. The one-photon absorption properties of NATSB on different metal surfaces were obtained by linear response calculations, as shown in Figure 3, where the averaged dipole strengths and excitation energies of the $S_0 \rightarrow S_1$ excitation are shown for different computational models. The dipole strength is equal to the squared norm of the transition dipole moment. The gray bars show the computed results of the NATSB chromophore in vacuum, which reflect the indirect effects of the environment (metal surface and solvent) on the geometry of NATSB and hence on the properties. The computed dipole strengths follow the order Au(111) in cyclohexane > Ag(111) in cyclohexane > Au(111) in water > Ag(111) in water, indicating that the indirect effect of Au(111) results in a larger dipole strength than that on Ag(111) surface and that the indirect effect of the highly polar water solvent leads to a smaller dipole strength compared with that in apolar cyclohexane. The inclusion of metal surfaces in QM/CMM calculations enhances the respective dipole strength owing to the direct effects on the electronic structure of NATSB, and such effects are more pronounced in the systems solvated in water. However, further inclusion of surrounding apolar or polar solvent molecules leads to almost negligible effects on the amplitude of the dipole strengths, indicating that the direct effects on dipole strengths mostly originate from the metal surfaces. A comparison between the metal surfaces and solvents suggests that the dipole strength is around 0.03 au larger on Au(111) surface than that on Ag(111) surface and that the dipole strength is around 0.05 au larger in cyclohexane than that in water. Figure 3 also shows the indirect effects on the excitation energies of NATSB, which lead to comparable results for all four systems. The inclusion of a metal surface in QM/CMM calculations, either Au(111) or Ag(111) surface, leads to a decrease in the excitation energy of around 0.07 eV owing to its direct effects on the electronic structure of NATSB. Further involvement of the cyclohexane solvent has no apparent effect on the excitation energies, while the presence of water molecules leads to a further decreased excitation energies. The absorption spectra of NATSB are thus red-shifted due to interaction with the metal surface and polar solvent molecules.

One- and Two-Photon Absorption. Calculations in vacuum reveal the influence of the geometrical relaxation of the molecule on the one- and two-photon absorption properties, which serves as an indirect effect in contrast to those direct effects on the electronic structure of the chromophore molecule. The computed one-photon absorption oscillator strengths and the two-photon absorption cross sections are shown in Figure 4. Note that the oscillator

dx.doi.org/10.1021/ct500579n | J. Chem. Theory Comput. XXXX, XXX, XXX−XXX

Table 1. Computed Transition Dipole Moment ($|\mu_{01}|$, in au), Difference between the Dipole Moment of Excited State and Ground State ($|\Delta\mu|$, in au), Angle between μ_{01} and $\Delta\mu$ ($\theta^{\mu_{01}}_{\Delta\mu}$, in deg), Excitation Energy (ΔE, in au), and Two-Photon Cross Section from the Two-State Model and from Quadratic Response Calculations (σ^{2SM} and σ^{TPA}, in GM)

metal	solvent	model	$\lvert\mu_{01}\rvert$	$\lvert\Delta\mu\rvert$	$\theta^{\mu_{01}}_{\Delta\mu}$	ΔE	σ^{2SM}	σ^{TPA}
Ag(111)	cyclohexane	NATSB	3.40	3.79	1.3	0.1271	296	221
Ag(111)	cyclohexane	NATSB + metal	3.45	4.24	1.3	0.1248	376	264
Ag(111)	cyclohexane	NATSB + metal + solvent	3.45	4.25	1.3	0.1248	378	265
Ag(111)	water	NATSB	3.13	3.20	2.4	0.1270	240	184
Ag(111)	water	NATSB + metal	3.33	4.01	1.4	0.1243	341	250
Ag(111)	water	NATSB + metal + solvent	3.34	4.43	1.4	0.1219	408	281
Au(111)	cyclohexane	NATSB	3.44	3.88	1.3	0.1269	320	231
Au(111)	cyclohexane	NATSB + metal	3.48	4.28	1.3	0.1247	389	270
Au(111)	cyclohexane	NATSB + metal + solvent	3.48	4.27	1.3	0.1247	388	270
Au(111)	water	NATSB	3.25	3.44	2.4	0.1265	263	199
Au(111)	water	NATSB + metal	3.38	4.06	1.5	0.1238	355	257
Au(111)	water	NATSB + metal + solvent	3.39	4.50	1.6	0.1204	424	295

strength is equal to 2/3 of the product of dipole strength and excitation energy (both in atomic units). We can see that in the system solvated in cyclohexane the metal surface and solvent molecules have negligible effects on the oscillator strengths of NATSB, which is ascribed to the fact that the environment actually puts opposite effects on the dipole strengths and excitation energies as shown in Figure 3. Since the oscillator strength is proportional to the product of the dipole strength and excitation energy, the consequence is that the environmental effects on the oscillator strength tend to cancel each other. In the case of water solvent, the involvement of metal surface leads to a slight increase in the oscillator strength due to stronger enhancement in the dipole strength; however, the oscillator is then suppressed by further involvement of water molecules in the QM/CMM calculations, since water is able to induce notable red-shift in the excitation energies (Figure 3). The overall effect of metal and solvent is that the averaged oscillator strength is larger in cyclohexane and that water leads to smaller oscillator strength by around 0.07.

We have also calculated the isotropic TPA cross section, namely the rotation-averaged TPA cross section of linearly polarized light according to the literature.[28] For the optimized geometry of NATSB in vacuum, quadratic response calculation gave a TPA cross section of 262 GM, which serves as a reference value to those obtained from instantaneous snapshots extracted from MD simulation trajectories (Figure 4, dashed line). The averaged TPA cross section over MD snapshots computed in vacuum (Figure 4, gray bars) suggests that polar and apolar solvents lead to a different TPA cross section owing to their different effects on the geometry of NATSB. In particular, geometrical relaxation of the molecule upon solvation in cyclohexane leads to a larger TPA cross section than that in water, although both are smaller than the reference TPA cross section for equilibrium geometry in vacuum (262 GM). This is in accordance with a previous study which reported that geometry relaxation in solvent diminishes the TPA cross section and that such effects are more pronounced in water than in cyclohexane.[16] However, when both metallic surface and solvent molecules are taken into account in the QM/CMM calculations, the TPA cross section in water becomes larger than the reference value, and such enhancement is more significant in water (Figure 4, cyan bars). This indicates that the direct polarization effect of metal surface and polar solvent molecules on the electronic structure of NATSB plays a dominant role over the indirect effect from geometry relaxation. Noteworthy, in the systems solvated in water the inclusion of metal substrate leads to a huge increase in the TPA cross section by around 60 GM (Figure 4, yellow bars), and further inclusion of surrounding water molecules offers an additional enhancement of around 35 GM. The effects of metal substrates in the systems solvated in cyclohexane are smaller (ca. 40 GM), and the apolar cyclohexane molecules have essentially negligible effect on the TPA cross section. Therefore, the linear conformation of NATSB in polar solvent (Figure 1) facilitates enhancement of the TPA cross section by metal substrates compared with the bent conformation in apolar solvent, despite the relatively larger distance between the molecule and metal surfaces. The combined effects of metal surface and water molecules further enhances the TPA, leading to larger TPA cross section than that in cyclohexane.

From the computed one-photon oscillator strength and two-photon absorption cross section we can see that the two metal surfaces have comparable effects on one- and two-photon absorption, although the effects arising from the Au(111) surface are slightly more pronounced than that of the Ag(111) surface. The solvent effects, however, are quite different for one- and two-photon absorption. The presence of apolar solvent results in larger oscillator strengths than water, while the TPA cross section is larger in polar solvent. Such contrastive behavior is interesting and originates from different effects of the environment on the optical properties. Due to the indirect effects from geometry relaxation of the NATSB molecule, the oscillator strengths and TPA cross sections both follow the order Au(111) in cyclohexane > Ag(111) in cyclohexane > Au(111) in water > Ag(111) in water (Figure 4, gray bars). The direct polarization effects from the metal surface and solvent molecules do not change the qualitative order of the oscillator strength; however, the influence on the TPA cross section is much more significant and leads to reversed order for polar and apolar solvents: Au(111) in water > Ag(111) in water > Au(111) in cyclohexane > Ag(111) in cyclohexane. From previous experience[26] it is inferred that the large enhancement of TPA cross section arises from the enlarged difference between the dipole moments of the excited state and the ground state, owing to the stronger polarization effects of the highly polar water molecules.

Two-State Model for Two-Photon Absorption. To figure out the origin of the enhancement in TPA cross section, we have performed analysis based on the two-state model (2SM),[29,30] which relates the transition dipole moment (μ_{01}),

dx.doi.org/10.1021/ct500579n | J. Chem. Theory Comput. XXXX, XXX, XXX−XXX

the difference between the dipole moments of the excited state and the ground state ($\Delta\boldsymbol{\mu}$), the angle between $\boldsymbol{\mu}_{01}$ and $\Delta\boldsymbol{\mu}$ ($\theta_{\Delta\boldsymbol{\mu}}^{\boldsymbol{\mu}_{01}}$), and the excitation energy (ΔE)

$$\delta^{2SM} = \frac{16}{15}\frac{|\boldsymbol{\mu}_{01}|^2|\Delta\boldsymbol{\mu}|^2}{\Delta E^2}(1 + 2\cos^2\theta_{\Delta\boldsymbol{\mu}}^{\boldsymbol{\mu}_{01}}) \quad (4)$$

Here $\Delta\boldsymbol{\mu} = \boldsymbol{\mu}_{11} - \boldsymbol{\mu}_{00} = \langle 1|\vec{\mu}|1\rangle - \langle 0|\vec{\mu}|0\rangle$ is computed from the double residue of the quadratic response function using the DALTON program package,[27] where 0 and 1 denote the ground state and the excited state, respectively. Note that all quantities in eq 4 are in atomic units, and δ^{2SM} is then converted to TPA cross section σ^{2SM} (in GM) using eq 3. The computed values are summarized in Table 1. The two-state model overestimates the TPA cross section by 30−45%; nonetheless, a nice linear correlation is found between σ^{2SM} and σ^{GM}, as shown in Figure 5, suggesting that the enhancement of

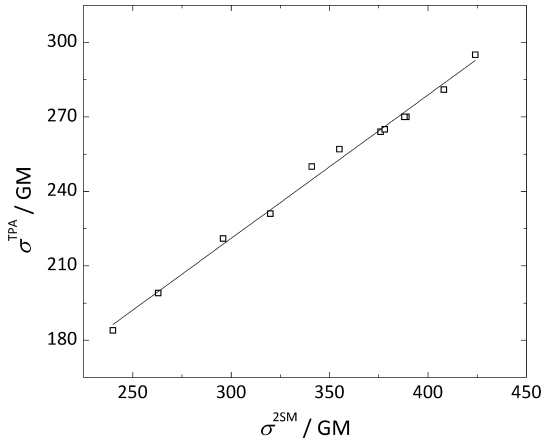

Figure 5. Linear correlation between the TPA cross sections from the two-state model and from quadratic response calculations.

two-photon absorption by metal surfaces and solvent molecules can be interpreted by the two-state model. According to the data listed Table 1, the transition dipole moment $|\boldsymbol{\mu}_{01}|$ is enhanced by around 5% owing to the direct polarization effects of the metal surface and solvent molecules. A much more significant enhancement arises from the difference between the dipole moments of excited state and ground state, $|\Delta\boldsymbol{\mu}|$. In cyclohexane $|\Delta\boldsymbol{\mu}|$ is enhanced by around 10% owing to the presence of metal surfaces, while in water this effect is around 20%. The presence of water molecules puts a further 10% enhancement in $|\Delta\boldsymbol{\mu}|$. Since δ^{2SM} is proportional to $|\Delta\boldsymbol{\mu}|^2$, such considerable enhancement in $|\Delta\boldsymbol{\mu}|$ overwhelms the unfavorable geometrical effect and eventually leads to a larger TPA cross section in water than that in cyclohexane (Figure 4).

It is known that the spatial overlap Λ between HOMO and LUMO is correlated with the amplitude of TPA cross section if the two frontier molecular orbitals contribute significantly to the two-photon excitation process.[7] The spatial overlap Λ ranges from 0 to 1 and reflects the character of the excitation: a small Λ indicates more charge transfer nature while a large Λ implies local excitation. In fact, for a specific organic chromophore, a larger Λ often indicates a more extended π-conjugation and hence a smaller HOMO−LUMO gap. We therefore plotted the relationship between the HOMO−LUMO gap and the TPA cross section, as shown in Figure 6. Here only the TPA cross sections obtained from the full model (NATSB + metal + solvent) are presented. One can see from Figure 6 that most points follow a linear correlation between HOMO−LUMO gap and TPA cross section; several outliers with rather low TPA cross section are also observed, and further investigation reveals that these outliers correspond to geometries of NATSB where the second lowest excited state (S_2, instead of S_1) contributes to a large TPA cross section. We can also see in Figure 6 that the HOMO−LUMO gap of NATSB is largely localized at higher values (4.8−5.6 eV) in apolar solvent, which is correlated with the lower TPA cross section (Figure 4). In polar solvent, the HOMO−LUMO gap of NATSB is narrowed, and this effect is more pronounced for the Au(111) surface.

Solvents versus Metal Surfaces. We have shown that the metal surfaces and the solvent molecules together offer a notable enhancement in the TPA cross section of physisorbed NATSB chromophore, and it is of interest to examine the respective contributions from the solvents and the metal surfaces. In fact, Figures 3 and 4 indicate that the contribution of the apolar cyclohexane to either one- or two-photon absorption is almost negligible, and we therefore focus on the effect of water molecules which is to be compared with those of the metal surfaces. Since Ag(111) and Au(111) in general show qualitatively the same behavior, we have chosen NATSB + Au(111) + water as a representative system and carried out

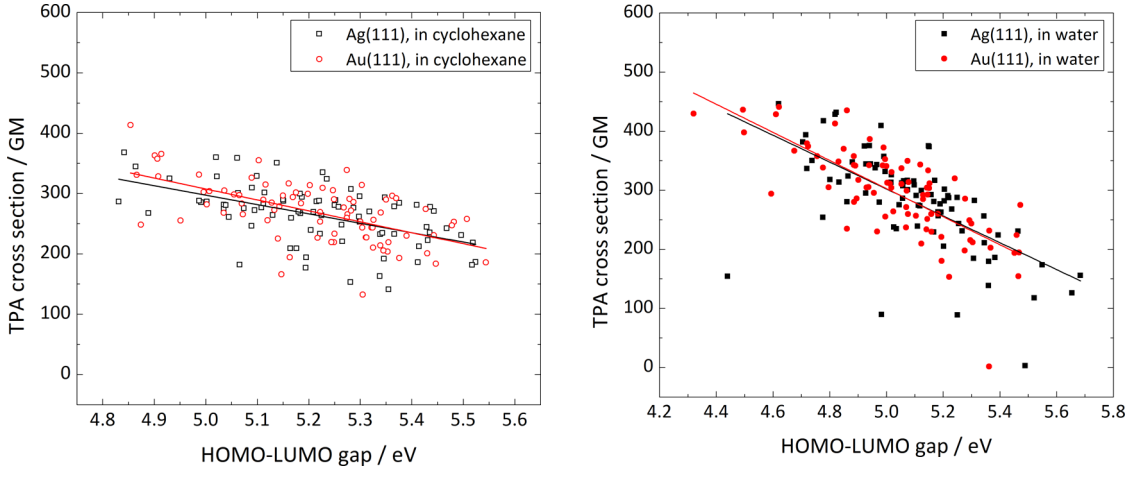

Figure 6. Linear correlation between the HOMO−LUMO gap and the TPA cross section.

dx.doi.org/10.1021/ct500579n | J. Chem. Theory Comput. XXXX, XXX, XXX−XXX

quadratic calculations of TPA cross sections of NATSB in solvent molecules, using the same snapshots as those extracted from the MD trajectories. Figure 7 shows the computed TPA

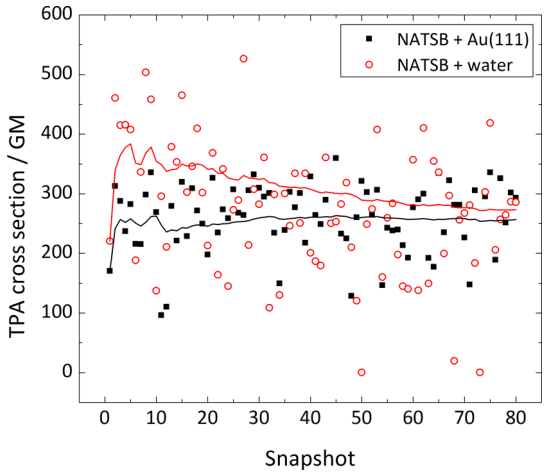

Figure 7. Computed TPA cross sections of NATSB with polarization effects from the metal surface and from solvent molecules, respectively.

cross sections of NATSB with gold surface and with water molecules, respectively. The solid lines are the running average over the 80 snapshots, from which it can be seen that both TPA cross sections are converging after averaging over 80 snapshots and that water has a slightly larger effect on TPA cross section than that of gold surface. Moreover, water molecules lead to a much broader distribution of the TPA cross sections. The averaged TPA cross section of NATSB with gold amounts to 257 GM, while that with water molecules is computed as 273 GM, both being notably larger than the result of NATSB in the absence of environmental effects (199 GM). The combination of water and gold surface offers an even larger TPA cross section of 295 GM, which is smaller than plain addition of the two enhancement effects, indicating a competition between the polarization effects between the metal surface and the polar solvent molecules.

Orientation-Dependence of Two-Photon Absorption. Since the NLO chromophores under investigation are adsorbed on planar metal surfaces, it is of interest to examine the dependence of TPA cross section on the orientation of the chromophore. According to the literature,[28] the amplitude of TPA is dependent on the polarization vectors of the two incoming photons. For simplicity, we here only consider the case of two photons with identical real polarization vectors, denoted as $\boldsymbol{\lambda}$, the direction of which can be described by spherical angles θ and φ. Here θ denotes the angle between $\boldsymbol{\lambda}$ and the z-axis, namely the normal direction of the metal surface, while φ represents the rotation of $\boldsymbol{\lambda}$ in the xy-plane, which is parallel to the metal surface. The observed TPA cross section for two identical incoming photons with polarization vector $\boldsymbol{\lambda}(\theta,\varphi)$ is given by[28]

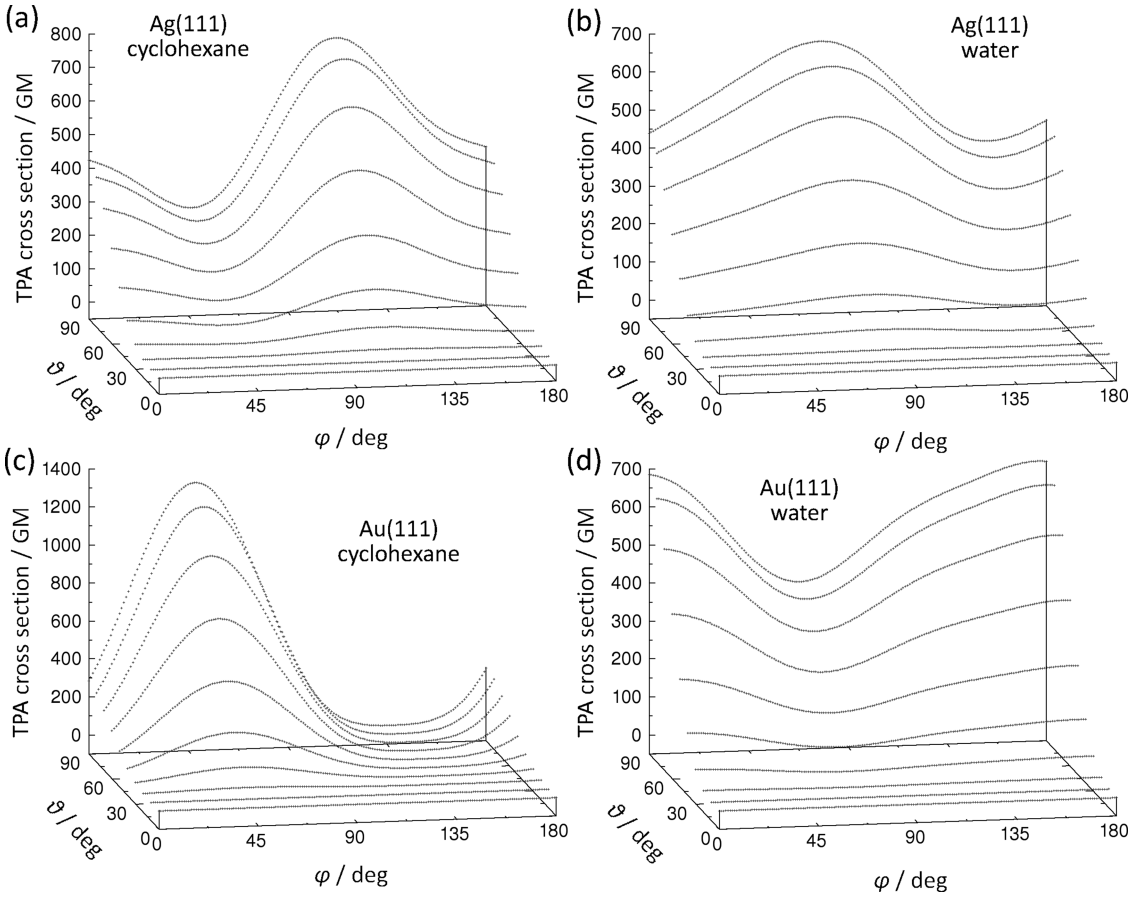

Figure 8. Dependence of two-photon absorption cross section on the polarization vector of the incident light for (a) NATSB on Ag(111) solvated in cyclohexane, (b) NATSB on Ag(111) solvated in water, (c) NATSB on Au(111) solvated in cyclohexane, and (d) NATSB on Au(111) solvated in water. θ and φ are spherical polar angles of the polarization vector.

dx.doi.org/10.1021/ct500579n | J. Chem. Theory Comput. XXXX, XXX, XXX−XXX

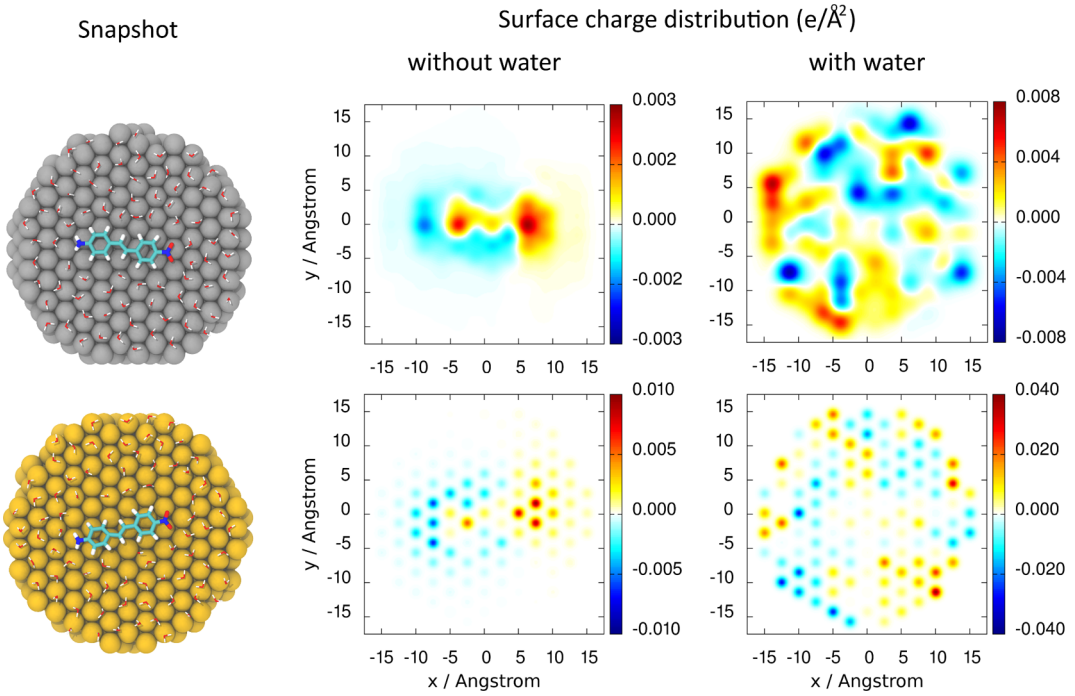

Figure 9. Snapshots and surface charge distributions of metal substrate (in $e/Å^2$) for NATSB (top) adsorbed on Ag(111) surface in aqueous solution and (bottom) adsorbed on Au(111) surface in aqueous solution. Only the first layer of solvent molecules is shown for clarity.

$$\delta(\theta, \varphi) = \sum_{\alpha\beta} \sum_{\xi\eta} \lambda_\alpha \lambda_\beta \lambda_\xi \lambda_\eta S_{\alpha\beta} S_{\xi\eta} \quad (5)$$

where α, β, ξ, and η denote Cartesian components, and $\boldsymbol{S}$ is the TPA transition amplitude tensor of the molecule. Note that the $\boldsymbol{S}$ tensor is computed in the laboratory coordinate system in which the orientation of the metal surface (instead of the chromophore molecule) is fixed, such that the transformation from the molecular coordinate system to the laboratory coordinate system is not needed. The Cartesian components of $\boldsymbol{\lambda}(\theta,\varphi)$ are expressed as $\{\sin\theta\cos\varphi, \sin\theta\sin\varphi, \cos\theta\}$, and the dependence of the observed TPA cross section on the spherical polar angles θ and φ can be feasibly obtained.

As shown in Figure 8, the observed amplitude of TPA cross section is almost zero when θ is zero, since the polarization vector is perpendicular to both the metal surface and the molecular plane of NATSB. As θ increases, the TPA cross section is enhanced and shows different patterns with respect to the φ angle, namely rotation of the chromophore in the xy-plane or the plane of the metal surface. A general trend is that the TPA cross section exhibits sharp maximum at certain φ angle in the apolar cyclohexane solvent, while in water the TPA cross section varies much more moderately with respect to φ. This is related to the limited lateral rotation of NATSB on the metal surface in cyclohexane, where the NATSB molecule is almost "anchored" on the Au(111) surface (Figure 2). The TPA cross section of the NATSB molecule adsorbed on Au(111) and solvated cyclohexane shows a sharp peak at around $\varphi = 45°$ where the polarization vector almost coincides with the long-axis of the molecule (Figure 8c). For NATSB adsorbed on Ag(111) and solvated in cyclohexane, the lateral rotation of the chromophore is slightly more free than that on Au(111), leading to a broader peak at around $\varphi = 120°$ (Figure 8a). In the presence of polar solvent, the amplitude of the TPA cross section shows less pronounced fluctuations with respect to φ, since the lateral rotation of the NATSB molecule around the normal direction of the metal surface is allowed (Figure 2).

Surface Charge Density Distribution on Metal Substrate. To shed light on the effects of the image charges of the metal substrate, we analyzed the surface charge distributions of the gold and silver surfaces. Since the most significant enhancement in TPA cross section was observed for chromophores adsorbed on metal surface in aqueous environment, we focus on the surface charge density distributions of metal surfaces in water to figure out how the TPA is enhanced. As shown in Figure 9, the induced point charge at each metal atom is represented by a Gaussian distribution according to Mayer[31] and contributes to the surface charge density distribution. Only the contributions from the surface layer are shown; the other two layers contribute negligibly to the surface charge densities. Owing to the larger capacitance parameter of silver (2.7529 au) than gold (1.2159 au),[13] the surface charges of the silver substrate delocalize with a larger Gaussian width, as reflected by the fact that the surface charges of silver substrate show a more continuous distribution over space while those of gold substrate behave more like discrete point charges. The maximal charge density on silver surfaces is therefore much smaller than those on gold surfaces. Nonetheless, the total amount of positive and negative charges on the silver surface are comparable (albeit smaller) than those on the gold surface. The accumulation of continuous distribution of net charges over large areas on silver surface compensates the low densities and leads to a comparable effect on the TPA cross section to that of gold surface.

In the absence of water molecules, the distributions of charge densities on silver and gold surfaces show some similarities. The positive charges are accumulated beneath the nitro group and the phenyl rings owing to their electron-rich character, while positive charges appear in the vicinity of the amine group and the aromatic hydrogen atoms. Such mirror-image-like charge distributions on metal surfaces arise from the almost-

dx.doi.org/10.1021/ct500579n | J. Chem. Theory Comput. XXXX, XXX, XXX−XXX

free motion of electrons in the metal substrate, which is effectively described by the capacitance−polarizability interaction model. The induced charges and dipoles on metal surfaces facilitate charge transfer of NATSB along the molecular long-axis owing to the charge separation pattern, and the relevant components of the TPA transition amplitude tensor are in turn enhanced. The difference between dipole moments of the excited state and the ground state, $|\Delta\mu|$, is also enhanced and leads to a larger TPA cross section according to eq 4.

The presence of water molecules complicates the induced charge densities on the metal surfaces, as shown in Figure 9. The interaction between water molecules and metal atoms leads to larger induced charges and dipoles compared with that from the NATSB chromophore. The positive and negative charges are respectively enriched at the sites where oxygen atoms and hydrogen atoms of water molecules are interacting with the metal surface. The stronger effects of water on the charge distribution of metal surface to some extent "dilute" the mirror-image charge of the NATSB molecule; still the combined effect of water and metal surface leads to an even larger enhancement of the components of the TPA transition amplitude tensor, as shown in Figure 10. In fact, the metal

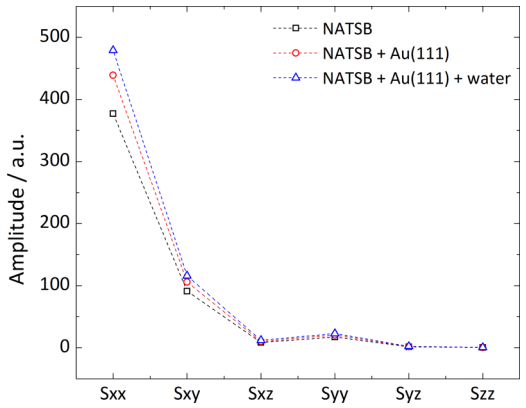

Figure 10. Cartesian components of the TPA transition amplitude tensor $\boldsymbol{S}$ computed from the snapshot shown in Figure 9.

surface and water molecules provide comparable enhancement in TPA cross section on their own (Figure 7), and they together provide further nonadditive enhancement in TPA cross section. Such TPA enhancement arises from the competing polarization effects from the metal surface and the polar solvent molecules and evokes the possibility of fine-tuning the TPA cross section of metal−assisted chromophore by choosing a proper solvent with optimal polarity and performance.

CONCLUSIONS

We have in this work extended the application of the multiscale quantum mechanical/capacitance molecular mechanical approach to two-photon absorption chromophores on metal surfaces. By analyzing the results of theoretical simulations with two types of solvent molecules and two types of metal surfaces, we can summarize our work in four points and in a general conclusion. First, there are salient environmentally induced structural changes of the adsorbates with consequences for the two-photon absorption−the 4-nitro-4′-amino-*trans*-stilbene chromophore adopts a bent conformation upon adsorption onto the metal surfaces in apolar solvent, while in the presence of polar solvent molecules the chromophore exhibits a slightly tilted linear conformation on the surfaces. The lateral rotation of the chromophore is sensitive to the type of solvent; in apolar solvent the chromophore shows highly restricted lateral rotation, while in polar solvent the molecule has much more freedom to rotate around the normal direction of the metal surface owing to diminished interaction between the chromophore and the metal surface. The second point of conclusion is that the presence of metal surfaces notably enhances the two-photon absorption cross section of the physisorbed chromophore, in our case by around 60 GM, and that the surrounding polar solvent molecules are able to further add to the enhancement of the two-photon absorption. The apolar solvent, however, induces only negligible effects on the two-photon absorption cross section. The third point concerns orientation-dependence of the two-photon absorption on surface, where we found that the two-photon absorption cross section is highly dependent on the spherical polar angle θ, namely the angle between the polarization vector of the incident light and the normal direction of the metal surface. When the lateral rotation of the adsorbed chromophore is restricted, the two-photon absorption also exhibits strong dependence on the spherical polar angle φ; the amplitude of two-photon absorption cross section reaches its maximum when the polarization vector of the incident light coincides with the long-axis of the chromophore. The fourth point of the conclusion is that the induced surface charge densities show a mirror-image-like pattern with respect to the adsorbates and are more localized and significant on gold surfaces than those on silver surfaces. The polar solvent molecules to some extent diminish the mirror-image charges of the chromophore on metal surfaces, still the two-photon absorption of the nonlinear optical chromophore is considerably enhanced by the combined and nonadditive enhancement effects from the metal surface and polar solvent molecules. Fine-tuning of the two-photon absorption is thus possible by choosing proper metal surfaces and solvents to achieve optimal performance. The general conclusion is that multiscale modeling offers a powerful tool for computer-aided design of metal−chromophore composite materials and constitutes a promising future development for tailoring nonlinear optical materials with desirable properties and performance.

ASSOCIATED CONTENT

Supporting Information

Refined CGenFF parameters of the NATSB molecule and comparison between the geometries and rotational barriers computed by QM and MM methods. This material is available free of charge via the Internet at http://pubs.acs.org.

AUTHOR INFORMATION

Corresponding Author

*E-mail: lixin@theochem.kth.se.

Notes

The authors declare no competing financial interest.

ACKNOWLEDGMENTS

We thank the Swedish National Infrastructure for Computing (SNIC) for providing computational resources for the project "Multiphysics Modeling of Molecular Materials", SNIC 2013/26-31.

■ ABBREVIATIONS

NLO, nonlinear optical; TPA, two-photon absorption; NATSB, 4-nitro-4′-amino-*trans*-stilbene; QM/CMM, quantum mechanics/capacitance molecular mechanics

■ REFERENCES

(1) Rinkevicius, Z.; Li, X.; Sandberg, J. A. R.; Mikkelsen, K. V.; Ågren, H. *J. Chem. Theory Comput.* **2014**, *10*, 989−1003.
(2) Li, X.; Rinkevicius, Z.; Ågren, H. *J. Phys. Chem. C* **2014**, *118*, 5833−5840.
(3) Rinkevicius, Z.; Li, X.; Sandberg, J. A. R.; Ågren, H. *Phys. Chem. Chem. Phys.* **2014**, *16*, 8981−8989.
(4) Pawlicki, M.; Collins, H. A.; Denning, R. G.; Anderson, H. L. *Angew. Chem., Int. Ed.* **2009**, *48*, 3244−3266.
(5) Lipparini, F.; Cappelli, C.; Barone, V. *J. Chem. Theory Comput.* **2012**, *8*, 4153−4165.
(6) Li, X.; Rinkevicius, Z.; Kongsted, J.; Murugan, N. A.; Ågren, H. *J. Chem. Theory Comput.* **2012**, *8*, 4766−4774.
(7) Murugan, N. A.; Apostolov, R.; Rinkevicius, Z.; Kongsted, J.; Lindahl, E.; Ågren, H. *J. Am. Chem. Soc.* **2013**, *135*, 13590−13597.
(8) Corni, S.; Tomasi, J. *J. Chem. Phys.* **2001**, *114*, 3739−3751.
(9) Jørgensen, S.; Ratner, M. A.; Mikkelsen, K. V. *J. Chem. Phys.* **2001**, *115*, 3792−3803.
(10) Neuhauser, D.; Lopata, K. *J. Chem. Phys.* **2007**, *127*, 154715.
(11) Arcisauskaite, V.; Kongsted, J.; Hansen, T.; Mikkelsen, K. V. *Chem. Phys. Lett.* **2009**, *470*, 285−288.
(12) Golze, D.; Iannuzzi, M.; Nguyen, M.-T.; Passerone, D.; Hutter, J. *J. Chem. Theory Comput.* **2013**, *9*, 5086−5097.
(13) Morton, S. M.; Jensen, L. *J. Chem. Phys.* **2010**, *133*, 074103.
(14) Payton, J. L.; Morton, S. M.; Moore, J. E.; Jensen, L. *Acc. Chem. Res.* **2013**, *47*, 88−99.
(15) Jensen, L. L.; Jensen, L. *J. Phys. Chem. C* **2008**, *112*, 15697−15703.
(16) Frediani, L.; Rinkevicius, Z.; Ågren, H. *J. Chem. Phys.* **2005**, *122*, 244104.
(17) Vanommeslaeghe, K.; Hatcher, E.; Acharya, C.; Kundu, S.; Zhong, S.; Shim, J.; Darian, E.; Guvench, O.; Lopes, P.; Vorobyov, I.; Mackerell, A. D. *J. Comput. Chem.* **2010**, *31*, 671−690.
(18) Wright, L. B.; Rodger, P. M.; Corni, S.; Walsh, T. R. *J. Chem. Theory Comput.* **2013**, *9*, 1616−1630.
(19) Hughes, Z. E.; Wright, L. B.; Walsh, T. R. *Langmuir* **2013**, *29*, 13217−13229.
(20) Brooks, B. R.; Brooks, C. L.; Mackerell, A. D.; Nilsson, L.; Petrella, R. J.; Roux, B.; Won, Y.; Archontis, G.; Bartels, C.; Boresch, S.; Caflisch, A.; Caves, L.; Cui, Q.; Dinner, A. R.; Feig, M.; Fischer, S.; Gao, J.; Hodoscek, M.; Im, W.; Kuczera, K.; Lazaridis, T.; Ma, J.; Ovchinnikov, V.; Paci, E.; Pastor, R. W.; Post, C. B.; Pu, J. Z.; Schaefer, M.; Tidor, B.; Venable, R. M.; Woodcock, H. L.; Wu, X.; Yang, W.; York, D. M.; Karplus, M. *J. Comput. Chem.* **2009**, *30*, 1545−1614.
(21) Bussi, G.; Donadio, D.; Parrinello, M. *J. Chem. Phys.* **2007**, *126*, 014101.
(22) Hess, B.; Kutzner, C.; van der Spoel, D.; Lindahl, E. *J. Chem. Theory Comput.* **2008**, *4*, 435−447.
(23) Yanai, T.; Tew, D. P.; Handy, N. C. *Chem. Phys. Lett.* **2004**, *393*, 51−57.
(24) Schäfer, A.; Huber, C.; Ahlrichs, R. *J. Chem. Phys.* **1994**, *100*, 5829−5835.
(25) Salek, P.; Vahtras, O.; Guo, J.; Luo, Y.; Helgaker, T.; Ågren, H. *Chem. Phys. Lett.* **2003**, *374*, 446−452.
(26) Murugan, N. A.; Kongsted, J.; Rinkevicius, Z.; Aidas, K.; Mikkelsen, K. V.; Agren, H. *Phys. Chem. Chem. Phys.* **2011**, *13*, 12506−12516.
(27) Aidas, K.; Angeli, C.; Bak, K. L.; Bakken, V.; Bast, R.; Boman, L.; Christiansen, O.; Cimiraglia, R.; Coriani, S.; Dahle, P.; et al. *WIREs Comput. Mol. Sci.* **2014**, *4*, 269−284.
(28) Monson, P. R.; McClain, W. M. *J. Chem. Phys.* **1970**, *53*, 29−37.
(29) Cronstrand, P.; Luo, Y.; Ågren, H. *Chem. Phys. Lett.* **2002**, *352*, 262−269.
(30) List, N. H.; Olsen, J. M. H.; Jensen, H. J. A.; Steindal, A. H.; Kongsted, J. *J. Phys. Chem. Lett.* **2012**, *3*, 3513−3521.
(31) Mayer, A. *Phys. Rev. B* **2007**, *75*, 045407.